PCCP

Accepted Manuscript

ROYAL SOCIETY OF CHEMISTRY

www.rsc.org/pccp

PCCP

RSCPublishing

ARTICLE

Cite this: DOI: 10.1039/x0xx00000x

Modeling the structure and thermodynamics of ferrocinium-based Ionic Liquids.

Carlos E. S. Bernardes,[a,*] Tomoyuki Mochida[b] and José. N. Canongia Lopes[a,c,*]

Received ooth January 2015,
Accepted ooth January 2015

DOI: 10.1039/x0xx00000x

www.rsc.org/

A new force-field for the description of ferrocinium-based ionic liquids is reported. The proposed model was validated by confronting Molecular Dynamics simulations results with available experimental data —enthalpy of fusion, crystalline structure and liquid density— for a series of 1-alkyl-2,3,4,5,6,7,8,9-octamethylferrocenium bis(trifluoromethylsulfonyl)imide ionic liquids, $[C_nFc][NTf_2]$ ($3 \leq n \leq 10$). The model is able to reproduce the densities and enthalpies of fusion with deviations smaller than 2.6% and 4.8 $kJ \cdot mol^{-1}$, respectively. The MD simulation trajectories were also used to compute relevant structural information for the different $[C_nFc][NTf_2]$ ionic liquids. The results show that, unlike other ILs, the alkyl side chains present in the cations are able to interact directly with the ferrocinium core of other ions. Even the ferrocinium charged cores (with relatively mild charge densities) are able to form small contact aggregates. This causes the partial rupture of the polar network and precludes the formation of extended nano-segregated polar-nonpolar domains normally observed in other ionic liquids.

1. Introduction

The unique properties of ionic liquids (ILs) include relatively large liquid temperature ranges, wide electrochemical windows, high chemical stability, non-flammability, high heat capacity, negligible vapour pressure, high storage density and the ability to solubilise an ample variety of solutes.[1, 2]

In recent years other chemical and physical properties started to be explored with the synthesis of ILs based on ions that include transition metals.[3-9] For example, the existence of paramagnetic metals can yield ILs with magnetic susceptibility[3, 4, 7, 9] or, because many metals can act as catalysts, the use of metal-based ILs can be explored in homogenous catalysis processes.[10, 11]

Little information about the structure at the molecular level of these new ILs is currently available. From a theoretical perspective, this reflects the absence of a force field adequate to perform relevant Molecular Dynamics (MD) simulations.

In this work we present a force field that models ILs based on different decamethylferrocenium cation derivatives, namely 1-alkyl-2,3,4,5,6,7,8,9-octamethylferrocenium ($[C_nFc]^+$; Fig. 1). This choice is justified by the availability of experimental data for the validation of the proposed model[12-14] and by the ability to investigate in a systematic way the effect of substituting the methyl groups in a pentamethylcyclopentadienyl ring with hydrogen atoms or alkyl chains of different size.

2. Theoretical Model and Simulations

Force Field Details. The force field for the $[C_nFc]$-based ionic liquids was developed in two stages: *i*) the establishment of an intramolecular parameterization capable of reproducing the structural features of the ferrocinium cation and its alkyl-substituted derivatives; and *ii*) the introduction of intermolecular parameters compatible with the models previously established for other IL families.[15]

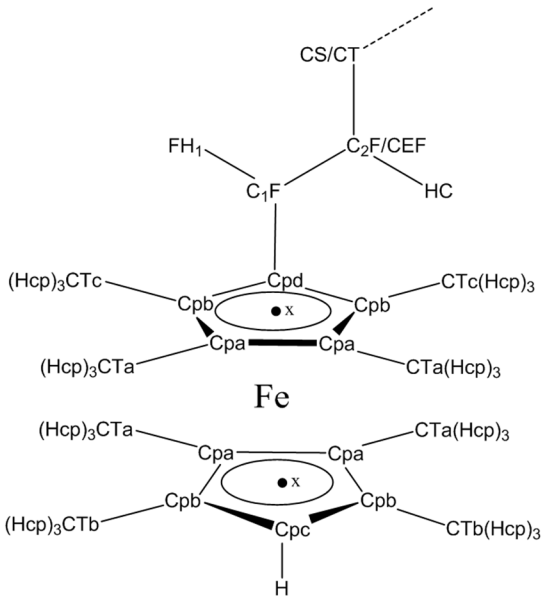

Fig. 1 Molecular structure of 1-alkyl-2,3,4,5,6,7,8,9-octamethylferrocenium cations $[C_nFc]^+$. The additional characters included in the designation of the carbon or hydrogen atoms follow the nomenclature adopted in the text.

The first stage comprises the description of the geometric characteristics of the cation (i.e. bond distances, angles and dihedrals); the second stage includes the determination of van der Waals parameters and atomic point charges for each interaction centre. The overall force field functional takes the form:[16]

$$U = \sum_{ij}^{\text{bonds}} \frac{k_{r,ij}}{2}\left(r_{ij} - r_{\text{o},ij}\right) + \sum_{ijk}^{\text{angles}} \frac{k_{\theta,ijk}}{2}\left(\theta_{ijk} - \theta_{\text{o},ijk}\right)^2 + \sum_{ijkl}^{\text{dihedrals}} \sum_{n=1}^{5} \frac{V_{n,ijkl}}{2}\left[1 + (-1)^n \cos\left(n\varphi_{ijkl}\right)\right] + \sum_i \sum_{j>i} \left\{ 4\varepsilon_{ij}\left[\left(\frac{\sigma_{ij}}{r_{ij}}\right)^{12} - \left(\frac{\sigma_{ij}}{r_{ij}}\right)^{6}\right] + \frac{q_i q_j}{4\pi\varepsilon_{\text{o}} r_{ij}} \right\} \quad (1)$$

where r_{ij}, θ_{ijk} and φ_{ijkl} are i–j distances, i–j–k angles and i–j–k–l dihedral angles, respectively, between interaction centres i, j, k and l. The o subscripts refer to equilibrium intramolecular distances and angles. The $k_{r,ij}$, $k_{\theta,ijk}$, and $V_{n,ijkl}$ parameters refer to bond and angle force constants (Fourier coefficients in the later case). Finally, σ_{ij} and ε_{ij} are 12-6 Lennard-Jones parameters, ε_o is the vacuum permittivity and q_i and q_j are atomic point charges.

Intramolecular Potential. The force field here presented for [C_nFc]-based cations, Table 1, was built from parameterizations previously reported for ferrocene-based molecules and ionic liquids.[15, 17, 18] All additional structural parameters in this work were taken from X-ray data available in the literature.[12, 14]

A particular feature of the [C_nFc] cations (Fig. 1), is the existence of two cyclopentadienyl rings in a "sandwich" configuration relative to the iron atom. The two rings in the structure have the ability to rotate one in relation to the other and, due to the symmetry of the interaction between the rings and the η_5 hybrid orbitals of the iron atom, the most stable configuration is found when the rings are eclipsed relative to each other (if substituent steric effects are ignored).[17] In the case of the ferrocene force field,[17, 18] this partially hindered internal rotation was modelled including massless dummy atoms (X) at the centre of mass of each ring and defining 25 C–X–X–C dihedral angles. In order to accommodate the two massless dummy atoms in the MD calculations, two rigid units containing the dummy atoms and the ten carbon atoms of the two rings were also defined. In this work, such procedure was also initially followed. However, it was observed that, as the number and size of the alkyl chains attached to a ring increased, the SHAKE algorithm used in the MD package DLPOLY[19] failed to converge. In order to overcome this problem, a small mass, 0.1 a.m.u., was transferred from each carbon atom of the ring to the dummy atom, so that the use of rigid units could be avoided. This mass transfer does not modify the centre of mass of the cation and, thus, it is not likely to change the dynamic properties of the cation. It is expected, however, a small modification of the moment of inertia of the rings, that should not influence significantly the simulation results. In order to keep the dummy atoms at the centre the mass of each ring and the two rings parallel to each other, we have stipulated (X–C) bonds and (C–X–X) angles with large force constants of $k_{r,ij}$ = 5000 kJ·mol^{-1} Å^{-2} and $k_{\theta,ijk}$ = 999.99 kJ·mol^{-1}·rad^{-2}, respectively. Finally, the iron atom was also kept between the two rings via strong harmonic bonds to the ring carbon atoms with force constants of $k_{r,ij}$ = 4500 kJ·mol^{-1} Å^{-2}. The avoidance of rigid units in the model makes it more general and probably enhances the chances of transferability to other MD simulation platforms other than DLPOLY.

Intermolecular Potential. The electrostatic interactions, as mentioned above, were modelled as atomic point charges (APCs). These were obtained following the methodology previously recommended for ferrocene compounds:[17] *i*) initially, a geometry optimization was performed at the B3PW91/SddAll [20-22] level of theory; *ii*) the obtained geometry was then used to compute the APCs by the ChelpG methodology, at the B3PW91/6-311G(3df,3pd) theoretical level.[20, 23, 24] All quantum calculations were performed using Gaussian 03.[25] The final APCs were obtained by averaging the results for all equivalent atoms found in $[C_3Fc]^+$ and $[C_4Fc]^+$.

Regarding the Lennard–Jones parameters, these were borrowed from the CL&P[15] and OPLS-AA force fields[16] or from the previously recommended parameters for ferrocene derivatives.[17, 18] In relation to the iron atom, the parameters previously recommended for Fe^{2+} were selected, even though, in the present case, the oxidation state of this atom is Fe^{3+}. This is expected to be a good approximation, since, as demonstrated before, within the same row of transition metals, the same parameters are transferable between adjoining atoms, disregarding their oxidation state.[26]

Validation Methodology/Details. The validation of the force field was performed evaluating the ability of the proposed parameterization to reproduce the reported crystalline structures and enthalpies of fusion of $[C_3Fc][Ntf_2]$ and $[C_4Fc][Ntf_2]$ and comparing the density of liquid $[C_6Fc][Ntf_2]$ and $[C_{10}Fc][Ntf_2]$ with the corresponding experimental values (cf. next section).

All MD simulations were perform using DL-POLY.[19] The parameterization of the bis(trifluoromethylsulfonyl)imide anion was previously reported.[27] The simulation boxes of the solid phases were prepared taking into account the dimension and occupancy of the unit cells of the experimental structures and stacking several unit cells to produce approximately cubic simulation boxes. In the case of the liquid phases, all simulations started from expanded simulation boxes where the cations and anions were randomly distributed. A cutoff distance of 1.6 nm and Ewald summations applied beyond this limit, were used in all simulations. Details of the simulation boxes sizes, composition, Ewald sum parameters and temperatures are given in Table 2. A pressure of 0.1 MPa was used in all simulations.

The anisotropic isothermal-isobaric ensemble (*N*-σ-*T*) was selected for the simulations of solid phases, while for liquids, the isotropic isothermal-isobaric ensemble (*N*-*P*-*T*) was used. The Nosé-Hoover thermostat and barostat with relaxation time constants of 0.1 ps and 0.5 ps, respectively, were applied in all simulations. A time step of 0.5 fs was selected for all MD runs. The simulation of the solid phase consisted of a 1 ns production stage, preceded by equilibration periods of 0.2 ns. As previously discussed,[26, 28, 29] because the initial configurations are close to equilibrium, these relatively short simulation times are adequate to complete the structure relaxation. In the case of the liquid phases, the equilibration was performed using several cycles where the temperature and pressure were changed consecutively, until a constant liquid density was obtained at the final temperature and pressure. The whole equilibration/production process lasted several tens of nanoseconds.[26]

Table 1. 1-Alkyl-2,3,4,5,6,7,8,9-octamethylferrocenium cation, $[C_nFc]^+$, force-field parameters. Nomenclature as in Fig. 1.

atoms	m / a.m.u.	q / a.c.u.	ε / kJ·mol^{-1}	σ / pm	ref.
X	0.500	0.00	0.0000	000	[f]
Fe	55.847	0.14[f]	1.2000	311	17
Cpa	11.911	0.01[f]	0.2930	355	17
Cpb	11.911	0.09[f]	0.2930	355	17
Cpc	11.911	−0.23[f]	0.2930	355	17
Cpd	11.911	−0.13[f]	0.2930	355	17
CTa	12.011	−0.15[f]	0.2761	350	17
CTb	12.011	−0.18[f]	0.2761	350	17
CTc	12.011	−0.23[f]	0.2761	350	17
Hcp	1.008	0.08[f]	0.1255	250	17
H	1.008	0.16[f]	0.1255	242	17
C_1F	12.011	0.09[f]	0.2761	350	17
H_1F	1.008	0.01[f]	0.1255	250	17
C_2F	12.011	−0.07[f]	0.2761	350	17
CEF	12.011	−0.13[f]	0.2761	350	30
CS	12.011	−0.12[f]	0.2761	350	30
CT	12.011	−0.18[f]	0.2761	350	30
HC	1.008	0.06[f]	0.1255	250	30

bonds	r_0 / pm	k_r / kJ·mol^{-1}.Å^{-2}	ref.	angles	θ_0 / deg	k_θ / kJ·mol^{-1}·rad^{-2}	ref.
X–Cp*[a]	122.5	5000.0	[f]	H*–C*–H*[c]	107.8	276.14	30
Cp*–Cp*[a]	144.0	3927.2	17,16	C*–C*–H*[c]	110.7	313.80	30
Fe–Cp*[a]	208.8	4500.0	[f]	C*–C*–C*[c]	112.7	488.30	16
Cp*–C_1F	151.0	2654.4	16	Cp*–Cp*–Cp*[a]	108.0	527.54	16, 17
Cp*–C*[b,c]	149.5	2845.0	17	Cp*–Cp*–C*[a,c]	126.0	586.10	17
Cpc–H	108.0	Constrained	17	Cp*–Cp*–H[a]	126.0	292.90	17
C*–H*[c]	109.0	Constrained	30	Cp*–C*–H*[a,c]	107.8	276.14	17
C*–C*[c]	152.9	2242.6	30	Cp*–C*–C*[a,c]	112.7	488.30	16
				Cp*–X–X[a]	90.0	999.99	[f]

Dihedrals[d]	V_1 / kJ·mol^{-1}	V_2 / kJ·mol^{-1}	V_3 / kJ·mol^{-1}	V_5 / kJ·mol^{-1}	ref.
–Cp–Cp*–*[e]	0.0000	44.9800	0.0000	0.0000	17
Cp*–X–X–Cp*[a]	0.0000	0.0000	0.0000	0.1440	17
Cp* Cp*–C*–H*[a,c]	0.0000	0.0000	0.5190	0.0000	17
C*–C*–Cp*–Cp*[a,c]	0.0000	0.0000	0.0000	0.0000	16
C*–C*–C*–Cp*[a,c]	7.2800	−0.6570	1.1670	0.0000	16
H*–C*–C*–Cp*[a,c]	0.0000	0.0000	1.9340	0.0000	16
C*–C*–C*–C*[c]	7.2800	−0.6569	1.1673	0.0000	30
C*–C*–C*–H*[c]	0.0000	0.0000	1.5313	0.0000	30
H*– C*–C*–H*[c]	0.0000	0.0000	1.3305	0.0000	30
–Cp–*–*[e,g]	0.0000	9.20480	0.0000	0.0000	16

[a] Cp* can be any Cpa, Cpb, Cpc or Cpd; [b] For CT, CTa, CTb or CTc; [c] C* and H* represent any generic aliphatic carbon (including C_1F) and hydrogen, respectively; [d] V_4 = 0.0 kJ·mol^{-1} for all dihedrals; [e] The asterisk represent any atom type; [f] This work (see text for details); [g] Improper dihedral.

The standard molar enthalpy of fusion of $[C_3Fc][Ntf2]$ and $[C_4Fc][Ntf_2]$ at the melting temperature was obtained from:

$$\Delta_{fus}H^\circ_m = U^\circ_{conf,\,m}(l) - U^\circ_{conf,\,m}(cr) + p\Delta V_m \qquad (2)$$

where $p = 10^5$ Pa is the ambient pressure, ΔV_m is the difference between the molar volume of the liquid and the solid, and $U^\circ_{conf,\,m}(l)$ and $U^\circ_{conf,\,m}(cr)$ are the configurational energies of the liquid and solid at the melting temperature, respectively.

3. Experimental Details

Density Measurements. In order to validate the model taking into consideration ferrocinium-based ILs with long alkyl side chains, the density of liquid $[C_6Fc][Ntf_2]$ and $[C_{10}Fc][Ntf_2]$ samples were measured experimentally. The two ionic liquids were produced and purified according to the synthetic routes and separation methodologies previously reported in the literature.[14]

The liquid densities were measured using an AccuPyc II 1340 pycnometer (Micromeritics Instrument Corporation) which optimum performance is at temperatures slightly below room temperature (cf. Tables 2 and 3). It must be stressed that the melting point temperature of $[C_6Fc][Ntf_2]$ (300.85 K) is greater than the temperature of the reported liquid density determination (296.75 K). Such determination was possible due to the fact that the ionic liquid enters very easily a liquid super-cooled regime. The resulting meta-stability allows the correct

thermal stabilization of the sample in the pycnometer and the determination of reliable liquid density values.

Table 2. Control parameters for the performed simulation runs.

Ionic Liquid	State	Ions Pairs	Ewald Parameters				T /K
			$k1$	$k2$	$k3$	α /pm	
$[C_3Fc][Ntf_2]$	cr	216	12	14	14	21.696	173.00[a] 340.55[b]
	l	200	13	13	13	21.696	340.55[b] 373.00[c]
$[C_4Fc][Ntf_2]$	cr	192	13	13	12	21.696	100.00[a] 307.55[b]
	l	200	13	13	13	21.696	307.55[b] 373.00[c]
$[C_5Fc][Ntf_2]$	l	200	14	14	14	21.696	373.00[c]
$[C_6Fc][Ntf_2]$	l	200	14	14	14	21.696	296.75[d] 373.00[c]
$[C_8Fc][Ntf_2]$	l	200	14	14	14	21.696	373.00[c]
$[C_{10}Fc][Ntf_2]$	l	200	21	21	21	27.137	296.95[d] 373.00[c]

[a] Experimental crystallographic data temperature; [b] Melting point temperature; [c] Common reference temperature for all simulations; [d] Experimental liquid density data temperature

4. Results and Discussion

Force Field Assessment Results. The force field developed for $[C_nFc]$-based ionic liquids was evaluated by studying its ability to reproduce the crystalline structures of $[C_3Fc][Ntf_2]$ and $[C_4Fc][Ntf_2]$, and the corresponding enthalpies of fusion. The MD results and the experimental data (liquid density measurements) obtained in this work are reported in

Table 3.

The agreement between the MD-computed and experimental crystalline structures is very good: at any given temperature, the maximum differences are 1 % and 2.6 % for the unit cell dimensions and solid densities, respectively.

The computed values for the enthalpy of fusion also agree with the experimental data within the corresponding determination errors: for $[C_3Fc][Ntf_2]$ and $[C_4Fc][Ntf_2]$ differences of 4.2 kJ·mol^{-1} and 2.9 kJ·mol^{-1}, respectively, were observed. The corresponding MD computation errors are 8.2 and 5.1 kJ·mol^{-1}.

The performance of the force field was also checked by the comparison between the MD-computed and experimental density of liquid $[C_6Fc][Ntf_2]$ and $[C_{10}Fc][Ntf_2]$. The experimental results, 1320 kg·m^{-3} for $[C_6Fc][Ntf_2]$ and 1263 kg·m^{-3} for $[C_{10}Fc][Ntf_2]$, are in excellent agreement with the computed densities, 1332 and 1255 kg·m^{-3}, respectively, with deviations smaller than 1%.

The reported volumetric and enthalpy of fusion MD data indicate that the developed force field is able to capture adequately the structural features present in $[C_nFc]$-based ionic liquid and the interactions between its composing ions.

$[C_nFc][Ntf2]$ liquid structure. One of the main characteristics of the $[C_nFc]^+$ cations is the sandwich configuration of the two cyclopentadienyl rings relative to the iron atom. As illustrated in Fig. 2 for $[C_4Fc]^+$, the positive charge of the cation is more or less evenly distributed: the +1.000 a.c.u positive charge is distributed among the iron atom and the several atoms that compose the rings (the carbon atoms of the ring plus the hydrogen, methyl or methylene groups directly attached to them). If one considers the decamethylferrocinium cation as a

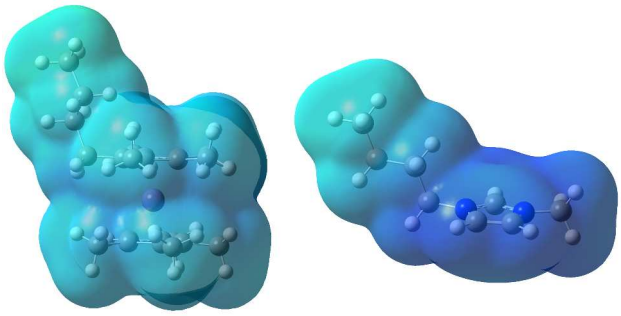

Fig. 2 Electrostatic potential mapped onto an electron density isosurface obtained at the B3PW91/6-311G(3df,3pd) level of theory, for $[C_4Fc]^+$ (left) and $[C_4C_1Im]^+$ (right). The colour code represents gradations from neutral charge densities (white) to positive charge densities (blue).

starting reference point, the charge distribution is +0.140 a.c.u. in the iron atom and +0.086 a.c.u in each of the ten C-CH_3 groups of the two rings. When a methyl group is replaced by an hydrogen atom, the new C-H group becomes slightly negative (–0.070 a.c.u.) and the remaining four C-CH_3 groups of that ring compensate this by becoming slightly more positive (+0.100 or +0.150 a.c.u.). On the other hand, when a methyl is replaced by a longer alkyl chain, the resulting C-CH_2-CH_2- group is slightly less positive (+0.030 a.c.u) and the remaining four C-CH3 groups on that ring accommodate the extra positive charge by becoming slightly more positive (+0.100 a.c.u.). This means that the charges on the two rings are similar, that the APCs that are placed on each atom are not very different from the APCs placed on neutral alkyl residues, and that the overall group charges are most of the time within the ±0.100 a.c.u range. This contrasts with the case of dialkylimidazolium-based cations, $[C_nC_mIm]^+$, where group charges can be as high as +0.200 a.c.u. (cf. Fig. 2) —a simple consequence of the fact that the charge is distributed only between 7 heavy atoms (one Im ring) instead of 20 (2 cyclopentdienyl rings plus adjoining atoms).

Given the charge distribution just described, it is expected that the interactions between the charged cores of the cations and between them and their alkyl side chains are more favourable in the case of ferrocinium-based ILs than in the case of ILs containing more traditional cations such as 1,3-dialkylimidazolium, N-alkylpyridinium, tetra-alkylammonium, or tetra-alkylphosphonium. Such difference can have a strong impact in the organization of the ions within the ionic liquids.

The existence of a polar network formed by the charged moieties of the ions that compose an ionic liquid can be probed by plotting radial distribution functions, $g(r)$s, between selected interactions centres representative of those moieties. These can be complemented by the calculation of Structure Factor functions, $S(q)$. The results are presented in Figs. 3 and 4.

In the case of $[C_nFc][Ntf_2]$ ionic liquids, the iron atom (Fe) of the cation and the nitrogen atom (NBT) of the anion are the obvious choices for the interaction centres of the charged moieties. The (Fe-NBT), (Fe-Fe) and (NBT-NBT) pair radial distribution functions are represented in Figs. 3(a) to 3(c).

The (Fe-Fe) rdfs in Fig. 3(b) show a sharp and intense first

peak that denote strong interactions between cations at shorter distances than the corresponding values for the anion-anion interactions —cf. Fig. 3(c). In fact, the first peak of the Fe-Fe $g(r)$ resembles more the first peak of the (Fe-NBT) interactions, Fig. 3(a), than that of Fig. 3(c). This sort of strong cation-cation interaction is absent in most traditional ILs.[31, 32]

Table 3. Comparison of simulated crystal structures (MD) and enthalpies of fusion with the corresponding experimental (Exp.) data in the literature[12, 14] and in this work.

Ionic Liquid	data	state	T / K	a / pm	b / pm	c / pm	α / deg	β / deg	γ / deg	V / nm^3	ρ / kg·m^{-3}	$\Delta\rho$ / %	$\Delta_{fus}H$ / kJ·mol^{-1}
$[C_3Fc][Ntf_2]$	Exp.	$C2/c$ cr.	173.00	163.89	189.44	192.62	90.0	113.2	90.0	5.497	1499	2.23	36.5[a]
	MD	$C2/c$ cr.	173.00	164.50	186.05	190.33	90.0	112.6	90.0	5.377	1533		–
	MD	$C2/c$ cr.	340.55	166.88	188.62	193.81	90.0	113.1	90.0	5.611	1469	–	41.3±8.2
	MD	liq.[b]	340.55	533.10	533.10	533.10	90.0	90.0	90.0	151.5	1360	–	
$[C_4Fc][Ntf_2]$	Exp.	$Pna2_1$ cr.	100.00	266.02	87.74	119.02	90.0	90.0	90.0	2.778	1517	2.59	26.5[a]
	MD	$Pna2_1$ cr.	100.00	262.04	86.96	118.82	90.0	90.0	90.0	2.708	1557		–
	MD	$Pna2_1$ cr.	307.55	266.30	88.38	121.34	90.0	90.0	90.0	2.856	1476	–	29.4±5.1
	MD	liq.[b]	307.55	533.10	533.10	533.10	90.0	90.0	90.0	152.8	1379	–	
$[C_6Fc][Ntf_2]$	Exp.	liq.	296.75	–	–	–	–	–	–	–	1320	0.91	–
	MD	liq.[b]	296.75	548.40	548.40	548.40	90.0	90.0	90.0	164.9	1332		–
$[C_{10}Fc][Ntf_2]$	Exp.	liq.	296.95	–	–	–	–	–	–	–	1263	–0.63	–
	MD	liq.[b]	296.95	575.00	575.00	575.00	90.0	90.0	90.0	190.2	1255		–

[a] measured at the melting point temperature; [b] the volumetric data correspond to cubic simulation boxes containing 200 ion pairs in the liquid phase.

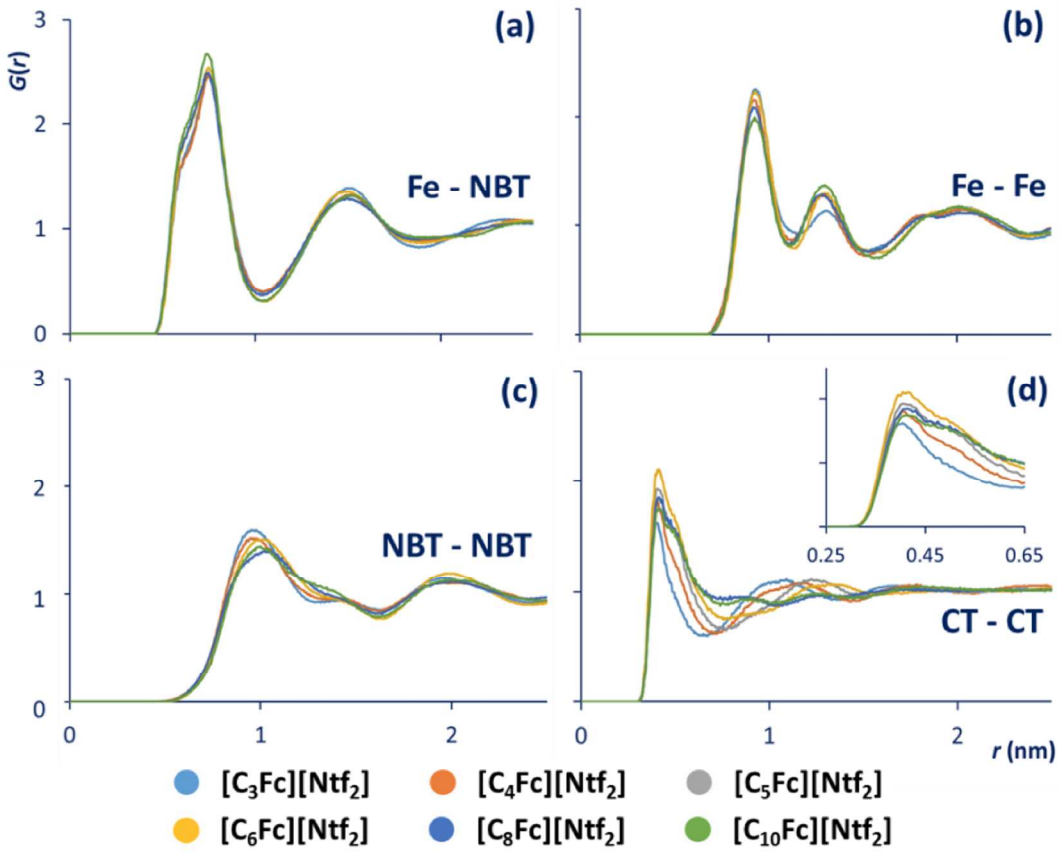

Fig. 3 Pair radial distribution functions, $g(r)$, for $[C_nFc][Ntf_2]$ ILs: (a) Fe-NBT $g(r)$s between the iron atom of the cation and the nitrogen atom of the anion; (b) Fe-Fe $g(r)$s; (c) NBT-NBT $g(r)$; (d) CT-CT $g(r)$s between the terminal carbon atoms of the cation alkyl chains. All simulation data were obtained at 373 K.

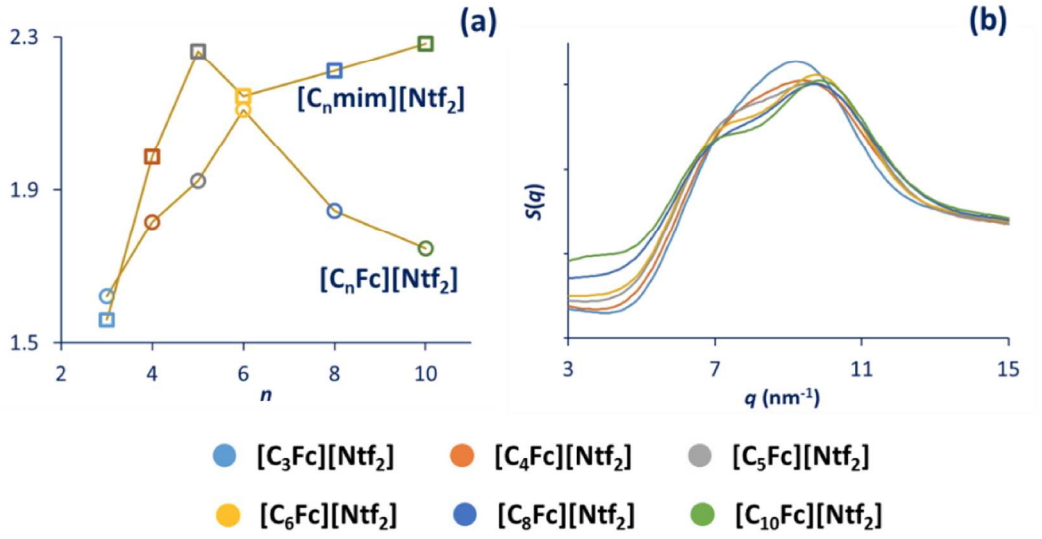

Fig. 4 (a) Intensity of the first peak of the CT-CT $g(r)$s of Fig. 3 as a function of n in [C$_n$Fc][Ntf$_2$] and [C_n*mim*][Ntf$_2$] ILs. (b) Total structure factor functions, $S(q)$, for [C$_n$Fc][Ntf$_2$] ILs. All simulation data were obtained at 373 K.

Furthermore, the difference of only 1.7 nm between the position of the first peaks in Fig. 3(a) and 3(b) is probably related with the large excluded volume caused by the two ferrocinium rings, that necessarily increases the separation between the iron atoms. However this does not prevent the formation of aggregates composed of adjoining cation cores, as seen in the simulation snapshots in Fig. 5 and in the spatial distribution functions in Fig. 6 (cf. discussion below).

The analysis of the pair radial distribution functions computed between the charged parts of the cation and anions, Fig. 3(a) to 3(c), shows that, in general, the increase of the cation alkyl chain does not significantly change the cation−anion, anion−anion and cation−cation interactions. This is also suggested from the inspection of the spatial distribution functions in Fig. 6 (left hand side), where it is observed that the arrangement of the anions around the cations is not significantly altered with the increase of the alkyl chains size. Fig. 6 also shows that the anions are mainly located between the cyclopentadyenyl rings or close to the rings centres of mass.

The effect of increasing the alkyl chain size in the structure of the nonpolar network was also investigated by computing the pair radial distribution functions between the terminal carbon atoms of the alkyl chains (CT), Fig. 3(d). The information obtained from those $g(r)$s is also complemented by the plots in Fig. 4(a) that represent the intensity of the first peak of the rdfs as a function of the alkyl side chain length, n, for [C$_n$Fc][Ntf2] and [C$_n$C$_1$Im][Ntf$_2$] ionic liquids. Fig. 3(d) reveals a strong interaction around 0.4 nm between the terminal carbon atoms of the alkyl chains. However, when the intensities of those peaks are compared with the ones obtained for [C$_n$mim][Ntf$_2$] a unexpected behaviour is found: in the case of imidazolium-based ILs, the intensity of the first peak of the CT-CT $g(r)$s increases up to n = 5 and then remains approximately constant; for [C$_n$Fc][Ntf2] ionic liquids, an intensity maximum is observed at n = 6, and similar intensities are found for n= 3 and n= 10. Such difference can be rationalized in terms of the more favourable interactions between the alkyl side chains and cation charged cores in the case of [C$_n$Fc][Ntf2] than in the case of [C$_n$C$_1$Im][Ntf$_2$]. The spatial distribution functions represented in the right side of Fig. 6 show a high probability of finding the terminal carbon atoms of the alkyl side chains close to the CP ring, around the methyl groups. As mentioned above, this specific interaction is related with the similarity between the APCs of the methyl groups connected to the cyclopentadienyl rings and those found in alkyl chains (Fig. 2 and Table 1). Longer chains are more flexible and will be able to interact more easily with the cation cores. This will lead to the non-monotonous behaviour in the [C$_n$Fc][Ntf$_2$] data in Fig. 4(a).

Another issue to be discussed in this context is the existence (or not) of nanosegregation between polar and nonpolar domains in [C$_n$Fc][Ntf$_2$] ionic liquids. 4(b) gives the total structure factor functions computed for these ILs. The inspection of the figure reveals the almost absence of peaks in the 2-4 nm^{-1} region (often called prepeaks) and only weak shoulder peaks around 7 nm^{-1}, thus suggesting the absence of nanosegregation —the formation of prepeaks is generally assigned to the existence of large and continuous nonpolar domains.[32, 33] As seen in the snapshots for [C$_3$Fc][Ntf$_2$] to [C$_6$Fc][Ntf$_2$] (Fig. 5(a) to 5(d)), the cations nonpolar groups are mainly isolated from each other or form small isolated aggregates. Only for [C$_8$Fc][Ntf$_2$] little chains of a nonpolar network starts to be observed and the percolation limit (the nonpolar aggregates start to coalesce and form a continuous sub-phase) is only observed for [C$_{10}$Fc][Ntf$_2$], giving rise to the small prepeak around 4 nm^{-1}, Fig. 4(b). The absence of pre-peaks (and their very mild appearance for chains above C8) finds an echo in imidazolium-based systems with functionalized side chains that are also able to interact with the cation cores.[31] Such chains are glyme-like polyether residues where every third carbon atom of an alkyl chain was replaced by a bridging oxygen atom. In such systems it was also found that prepeaks are present only for chains containing six carbon and three oxygen atoms.

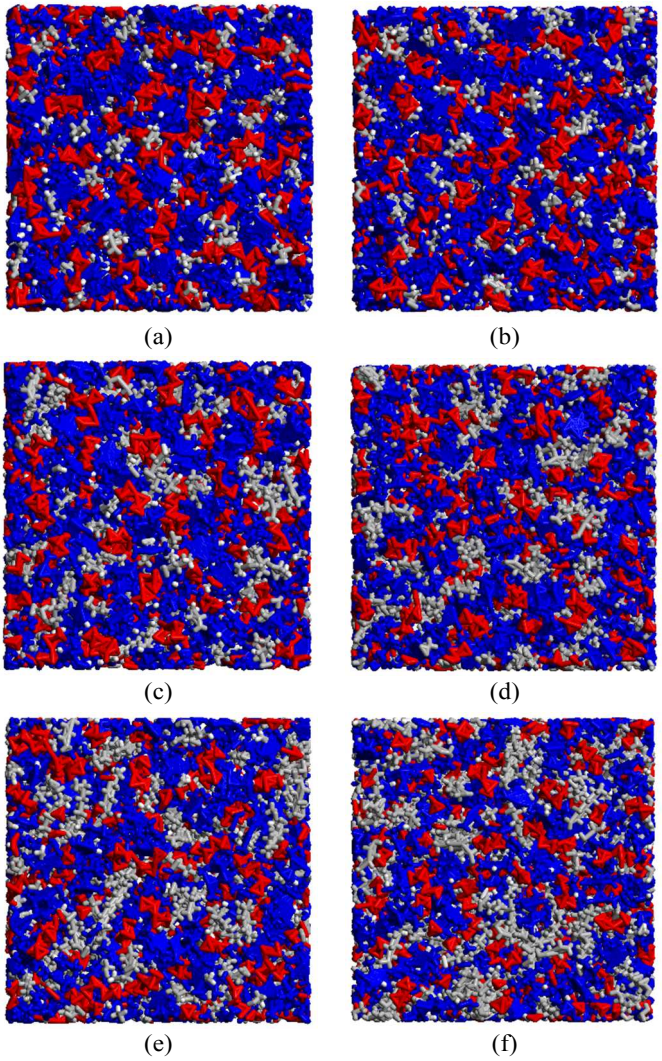

Fig. 5 MD simulation snapshots color-coded to reflect the presence of the charged parts of the cations (blue), the anions (red), and the alkyl side chains of the cations (gray). a) $[C_3Fc][Ntf_2]$; b) $[C_4Fc][Ntf_2]$; c) $[C_5Fc][Ntf_2]$; d) $[C_6Fc][Ntf_2]$; e) $[C_8Fc][Ntf_2]$; f) $[C_{10}Fc][Ntf_2]$. All results correspond to molecular simulations performed at 373 K.

Finally, and unlike conventional ILs, the $S(q)$ intermediate peaks are also extremely subdued. These peaks (also known as charge ordering peaks, COPs) are associated with the existence in the ILs of a polar network formed by the charged moieties of the cations and anions, characterized by alternating sequences of ions and counter-ions. Such distribution is an hallmark of most ionic liquids and causes the existence of prominent COPs.[31-33] The absence of well-defined COPs (and the corresponding polar networks) for $[C_nFc][Ntf_2]$ ionic liquids with $n < 6$, is probably related to the possibility of interactions between adjoining cations and the formation of cation-cation aggregates. Such structures lead to the breach of the alternating character of the polar network. As the alkyl chain is increased for $n \geq 6$, due to the increasing volume of the nonpolar groups, the polar network begins to be stretched and the formation of cation aggregates begins to be less favourable. This boosts the alternating character of the polar network and, thus, the appearance of intermediate shoulder peaks around 7 nm^{-1}, Fig. 4(b).

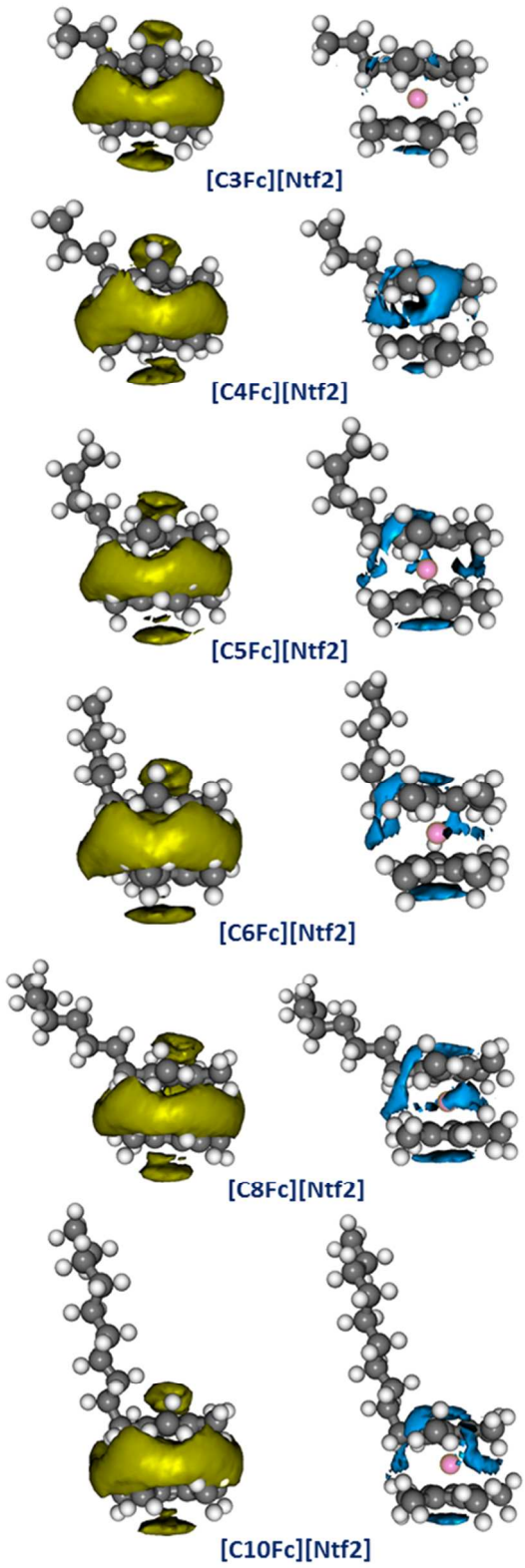

Fig. 6 Spatial distribution functions (SDFs) of the anions (left) and terminal carbon atoms of the cations alkyl chains (right) around the different alkyloctamethylferrocenium cations investigated in this work. All results correspond to molecular simulation performed at 373 K.

5. Conclusions

The proposed force field for alkyloctamethylferrocenium based ionic liquids was found to accurately reproduce the structural features of the crystal structure of $[C_3Fc][Ntf_2]$ and $[C_4Fc][Ntf_2]$ and the corresponding enthalpies of fusion. Furthermore, the liquid density of $[C_6Fc][Ntf_2]$ and $[C_{10}Fc][Ntf_2]$ were also accurately captured by the proposed model. It also shows a good degree of compatibility and transferability with previous parameterizations proposed for ionic liquids.

The nanostructure analysis of the $[C_nFc][Ntf_2]$ family of ionic liquids, revealed that, due to the electrostatic similarity between the methyl groups connected to the CP rings and that observed for nonpolar alkyl chains, the interactions between the different moieties of the cations (positively charged core, alkyl side chains) are much more favourable than for cations found on more traditional ionic liquids. This leads to the formation of cation-cation aggregates and the partial rupture of the polar network of the ferrocinium-based ionic liquids. One can always speculate that these differentiated structural features will have some consequences in terms of the dynamical properties of the ionic liquids that, combined to their unique electric, magnetic or catalytic properties, will open new opportunity windows for their use as novel media.

Acknowledgements

Financial support provided by Fundação para a Ciência e Tecnologia (FCT) through projects PTDC/QUI-QUI/116847/2010, FCT-ANR/CTM-NAN/0135/2012, PTDC/CTM-NAN/121274/2010 and PEst-OE/QUI/UI0100/2013.

Notes and references

[a] Centro de Química Estrutural, Instituto Superior Técnico, Universidade de Lisboa, 1049-001 Lisboa, Portugal.

* *E-mail: carlos.bernardes@tecnico.ulisboa.pt; jnlopes@ist.utl.pt*

[b] Department of Chemistry, Graduate School of Science, Kobe University, Kobe, Hyogo 657-8501, Japan.

[c] Instituto de Tecnologia Química e Biológica, Universidade Nova de Lisboa, 2580-157 Oeiras, Portugal.

1. H. Weingäertner, *Angew. Chem. Int. Ed.*, 2008, **47**, 654-670.
2. K. E. Johnson, *Electrochem. Soc. Interface*, 2007, **16**, 38-41.
3. S. Hayashi and H. O. Hamaguchi, *Chem. Lett.*, 2004, **33**, 1590-1591.
4. Y. Yoshida, A. Otsuka, G. Saito, S. Natsume, E. Nishibori, M. Takata, M. Sakata, M. Takahashi and T. Yoko, *Bull. Chem Soc Jpn*, 2005, **78**, 1921-1928.
5. P. Nockemann, B. Thijs, N. Postelmans, K. Van Hecke, L. Van Meervelt and K. Binnemans, *J. Am. Chem. Soc.*, 2006, **128**, 13658-13659.
6. B. Mallick, B. Balke, C. Felser and A. V. Mudring, *Angew Chem Int Edit*, 2008, **47**, 7635-7638.
7. T. Peppel, M. Köckerling, M. Geppert-Rybczynska, R. V. Ralys, J. K. Lehmann, S. P. Verevkin and A. Heintz, *Angew. Chem. Int. Ed.*, 2010, **49**, 7116-7119.
8. B. M. Krieger, H. Y. Lee, T. J. Emge, J. F. Wishart and E. W. Castner, *Phys. Chem. Chem. Phys.*, 2010, **12**, 8919-8925.
9. C. Guerrero-Sanchez, T. Lara-Ceniceros, E. Jimenez-Regalado, M. Rasa and U. S. Schubert, *Adv. Mater.*, 2007, **19**, 1740-1747.
10. G. Clavel, J. Larionova, Y. Guari and C. Guerin, *Chem. Eur. J.*, 2006, **12**, 3798-3804.
11. K. Bica and P. Gaertner, *Org. Lett.*, 2006, **8**, 733-735.
12. Y. Funasako, T. Mochida, T. Inagaki, T. Sakurai, H. Ohta, K. Furukawa and T. Nakamura, *Chem Commun*, 2011, **47**, 4475-4477.
13. T. Inagaki, T. Mochida, M. Takahashi, C. Kanadani, T. Saito and D. Kuwahara, *Chem. Eur. J.*, 2012, **18**, 6795-6804.
14. Y. Funasako, T. Inagaki, T. Mochida, T. Sakurai, H. Ohta, K. Furukawa and T. Nakamura, *Dalton Trans.*, 2013, **42**, 8317-8327.
15. J. N. Canongia Lopes and A. A. H. Padua, *Theor. Chem. Acc.*, 2012, **131**, 1129.
16. W. L. Jorgensen, D. S. Maxwell and J. Tirado-Rives, *J. Am. Chem. Soc.*, 1996, **118**, 11225-11236.
17. J. N. Canongia Lopes, P. C. Couto and M. E. Minas da Piedade, *J. Phys. Chem. A*, 2006, **110**, 13850-13856.
18. C. M. Lousada, S. S. Pinto, J. N. Canongia Lopes, M. F. M. Piedade, H. P. Diogo and M. E. Minas da Piedade, *J. Phys. Chem. A*, 2008, **112**, 2977-2987.
19. W. Smith and T. R. Forester, *The DL_POLY Package of Molecular Simulation Routines (v.2.2); The Council for The Central Laboratory of Research Councils*, Daresbury Laboratory, Warrington, 2006.
20. A. D. Becke, *J. Chem. Phys.*, 1993, **98**, 5648-5652.
21. T. Leininger, A. Nicklass, H. Stoll, M. Dolg and P. Schwerdtfeger, *J. Chem. Phys.*, 1996, **105**, 1052-1059.
22. T. H. Dunning, Jr. and P. J. Hay, *Modern Theoretical Chemistry*, Plenum, New York, 1976.
23. J. P. Perdew and Y. Wang, *Phys. Rev. B*, 1992, **45**, 13244-13249.
24. A. D. Mclean and G. S. Chandler, *J. Chem. Phys.*, 1980, **72**, 5639-5648.
25. M. J. Frisch, G. W. Trucks, H. B. Schlegel, G. E. Scuseria, M. A. Robb, J. R. Cheeseman, J. Montgomery, J. A., T. Vreven, K. N. Kudin, J. C. Burant, J. M. Millam, S. S. Iyengar, J. Tomasi, V. Barone, B. Mennucci, M. Cossi, G. Scalmani, N. Rega, G. A. Petersson, H. Nakatsuji, M. Hada, M. Ehara, K. Toyota, R. Fukuda, J. Hasegawa, M. Ishida, T. Nakajima, Y. Honda, O. Kitao, H. Nakai, M. Klene, X. Li, J. E. Knox, H. P. Hratchian, J. B. Cross, V. Bakken, C. Adamo, J. Jaramillo, R. Gomperts, R. E. Stratmann, O. Yazyev, A. J. Austin, R. Cammi, C. Pomelli, J. W. Ochterski, P. Y. Ayala, K. Morokuma, G. A. Voth, P. Salvador, J. J. Dannenberg, V. G. Zakrzewski, S. Dapprich, A. D. Daniels, M. C. Strain, O. Farkas, D. K. Malick, A. D. Rabuck, K. Raghavachari, J. B. Foresman, J. V. Ortiz, Q. Cui, A. G. Baboul, S. Clifford, J. Cioslowski, B. B. Stefanov, G. Liu, A. Liashenko, P. Piskorz, I. Komaromi, R. L. Martin, D. J. Fox, T. Keith, M. A. Al-Laham, C. Y. Peng, A. Nanayakkara, M. Challacombe, P. M. W. Gill, B. Johnson, W. Chen, M. W. Wong, C. Gonzalez and J. A. Pople, *Gaussian 03, Revision C.02*, Gaussian, Inc., Wallingford, 2004.
26. C. E. S. Bernardes, J. N. C. Lopes and M. E. Minas da Piedade, *J. Phys. Chem. A*, 2013, **117**, 11107-11113.
27. J. N. Canongia Lopes and A. A. H. Padua, *J Phys Chem B*, 2004, **108**, 16893-16898.
28. C. E. S. Bernardes, M. E. Minas da Piedade and J. N. Canongia Lopes, *J Phys Chem B*, 2012, **116**, 5179-5184.
29. R. G. Simões, C. E. S. Bernardes and M. E. Minas da Piedade, *Cryst. Growth Des.*, 2013, **13**, 2803-2814.
30. J. N. Canongia Lopes, J. Deschamps and A. A. H. Padua, *J Phys Chem B*, 2004, **108**, 2038-2047.
31. K. Shimizu, C. E. Bernardes, A. Triolo and J. N. Canongia Lopes, *Phys. Chem. Chem. Phys.*, 2013, **15**, 16256-16262.
32. C. E. S. Bernardes, K. Shimizu, A. I. M. C. L. Ferreira, L. M. N. B. F. Santos and J. N. Canongia Lopes, *J Phys Chem B*, 2014, **118**, 6885-6895.
33. K. Shimizu, C. E. S. Bernardes and J. N. Canongia Lopes, *J Phys Chem B*, 2014, **118**, 567-576.

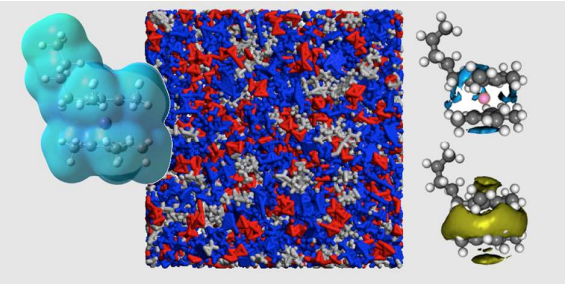

A new force-field for the description of ferrocinium-based ionic liquids is reported. Their unique nanostructure is probed by MD simulations.